NANO LETTERS

pubs.acs.org/NanoLett

Fast and Scalable Printing of Large Area Monolayer Nanoparticles for Nanotexturing Applications

Sangmoo Jeong,[†] Liangbing Hu,[‡] Hye Ryoung Lee,[†] Erik Garnett,[‡] Jang Wook Choi,[‡] and Yi Cui*,[‡]

[†]Department of Electrical Engineering and [‡]Department of Materials Science and Engineering, Stanford University, Stanford, California 94305

ABSTRACT Recently, there have been several studies demonstrating that highly ordered nanoscale texturing can dramatically increase performance of applications such as light absorption in thin-film solar cells. However, those methods used to make the nanostructures are not compatible with large-scale fabrication. Here we demonstrate that a technique currently used in roll-to-roll processing to deposit uniform thin films from solution, a wire-wound rod coating method, can be adapted to deposit close-packed monolayers or multilayers of silica nanoparticles on a variety of rigid and flexible substrates. Amorphous silicon thin films deposited on these nanoparticle monolayers exhibit 42% higher absorption over the integrated AM 1.5 spectrum than the planar controls. This simple assembly technique can be used to improve solar cells, fuel cells, light emitting diodes and other devices where ordered nanoscale texturing is critical for optimal performance.

KEYWORDS Nanotexture, printing, roll-to-roll, light trapping, nanoparticle

Nanotexturing a substrate is an important means to enhance many physical and chemical functions. For example, nano- and microwires,[1−3] nanocone,[4−6] nanodome,[7] and nanopillar[8] substrates have been shown to have effective broad-band antireflection and light trapping effects. Texturing at the nanoscale also can make substrates superhydrophobic or superhydrophilic, depending on the surface chemistry.[9] Recently, some research groups demonstrated adhesives mimicking gecko foot-hair by fabricating micro/nanofiber array texturing.[10,11] Thus far, the methods used to produce nanotextured surfaces include electron-beam lithography[10] and vapor−liquid−solid growth of nanowires or nanopillars,[1,2,8] and either Langmuir−Blodgett deposition,[12,13] spin coating,[14] or dip coating[3,12] to form a nanoparticle monolayer. These methods are useful for fundamental studies but are not easily scaled to large areas with fast and low-cost processing.

In this study, we develop a scalable and simple coating method for assembling silica nanoparticles on both rigid and flexible substrates that can directly be transferred to large-scale roll-to-roll processing. Our method is based on the wire-wound rod coating method, which deposits an even amount of fluid over a moving surface and is used to manufacture office products and flexible packaging.[15] We extend this technique to nanoparticle colloids to produce controllably two- and three-dimensional (2D and 3D) arrays of silica nanoparticles. We also studied several key parameters including contact angle, evaporation rate, viscosity, and nanoparticle concentration to understand the assembly mechanism. We demonstrated that the nanotextured morphologies generated by this simple coating method can be used as substrates to increase light absorption dramatically in thin amorphous silicon (a-Si:H) films, which is important for solar cell applications. We also demonstrated enhanced hydrophobicity using these nanotextured substrates.

Silica nanoparticles used in this study were synthesized by a modified Stober process.[16] A silica nanoparticle ink was prepared by mixing the nanoparticles with poly-4-vinylphenol (PVPh, Sigma-Aldrich) in ethanol. The typical concentrations of nanoparticles and PVPh were 50 g/L and 0.2% by weight, respectively. The coating assembly consisted of a wire-wound rod, which is a stainless steel rod with stainless steel wire wound around it. The nanoparticle ink was dropped onto the substrate and the rod was pulled across, leaving behind a volume of solution equal to the groove space between each wire winding and ultimately leading to a uniform film (Figure 1a). The diameter of the wire on the rod determines the thickness of the wet film. We typically used a rod (RD Specialties, Inc.) designed to make a 20.57 μm thick wet film. To improve uniformity, the rod was pulled with an automatic applicator at a speed of 0.8 cm/s. Figure 1b shows an optical image of a flexible plastic, poly(ethylene terephthalate) (PET) substrate (30 cm^2), which is fully covered with a close-packed silica nanoparticle monolayer fabricated by this process. The monolayer coverage is highly uniform across the whole substrate. We believe that this monolayer coating method can be applied to industrial scale applications.

* To whom correspondence should be addressed, yicui@stanford.edu.
Received for review: 04/23/2010
Published on Web: 07/14/2010

DOI: 10.1021/nl101432r | *Nano Lett.* **2010,** *10,* 2989–2994

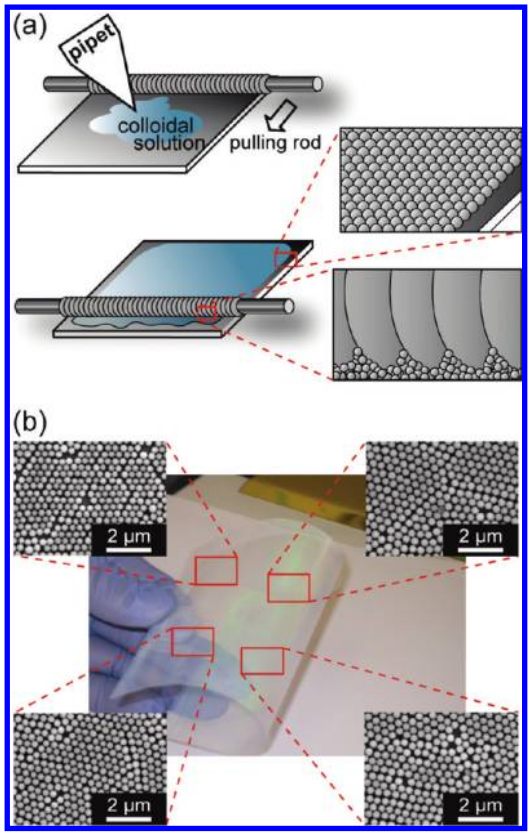

FIGURE 1. (a) Schematic illustration of a wire-wound rod coating method for printing nanoparticle monolayer. (b) An optical image of a close-packed silica nanoparticle monolayer printed by the wire-wound rod coating method on a flexible poly(ethylene terephthalate) (PET) substrate. Four insets show SEM images of the monolayer on different spots.

Since the assembly process occurs during the drying step, several parameters such as contact angle, evaporation rate, viscosity, and nanoparticle concentration play a critical role in achieving close-packed nanoparticle arrays over large areas. The first condition required to form high-quality films is that the ink completely wets the substrate. Once the nanoparticle ink is spread evenly by the wire-wound rod and wets the substrate, the solvent starts to evaporate gradually from the part where it was spread first. With the appropriate nanoparticle concentration, the particle-to-particle distance can be controlled such that when the solvent layer becomes as thin as the nanoparticle diameter, the solvent can remain between nanoparticles in the form of a meniscus. The meniscus provides a capillary force,[17,18] which drives the particles together, nucleating a thin film assembly. This nucleate grows from the convective flux of nanoparticles toward the drying front of the wet film.[19,20] Figure 2a illustrates this assembly mechanism. The ink, a mixture of nanoparticles and PVPh in ethanol, wets silicon and PET substrates completely. Even as the concentration of PVPh in ethanol increases from 0.2 to 10% by weight, its contact angle still remains close to zero. The PVPh is added to decrease the evaporation rate and increase the viscosity. When the concentration of the PVPh in the nanoparticle ink is in the range of 0.1−0.5% by weight, a monolayer is easily fabricated over a large area. However, with a higher concentration of PVPh, nanoparticles do not pack closely, because the PVPh forms a thick layer around the nanoparticles and prevents the assembly of a monolayer (Figure S1e and S1f, Supporting Information). If the solvent is too volatile or its viscosity is too low, instabilities in the array growth may arise and the wet film can easily break into separated droplets.[20,21] Table 1 summarizes the evaporation rate and the viscosity of solvents with different concentrations of PVPh. The increase of PVPh concentration as the solvent evaporates provides lower evaporation rate and higher viscosity. The 2D nanoparticle islands start to form around drying edges of the ink, and the controlled evaporation rate and viscosity by PVPh helps them to grow into a monolayer. Panels b and c of Figure 2 are scanning electron microscopy (SEM) images of resulting nice monolayers of nanoparticles formed when using PVPh. Without PVPh, rapid evaporation and low viscosity result in the breaking of liquid film and empty space between nanoparticle islands, as illustrated in Figure 2d, because nanoparticles from the convective flux do not have enough time to align into already-formed 2D islands. As shown in SEM images of panels e and f of Figure 2, the nanoparticle films were not continuous. Similar results are demonstrated when the PVPh concentration is lower than 0.1% (Figure S1a and Figure S1b, Supporting Information).

In order to test a wider range of parameters, we substituted a low vapor pressure liquid for PVPh in the nanoparticle ink and repeated the coating experiments. The ink was prepared with the same concentration of nanoparticles, 50 g/L, in a 1:1 mixture of ethanol and ethylene glycol (EG). Due to the lower vapor pressure (0.06 mmHg at 20 °C) of EG compared with that of ethanol (44 mmHg at 20 °C), the overall evaporation rate of the ink dramatically decreased, as listed in Table 1. Also, the viscosity increased by more than a factor of 6 compared to the mixture of ethanol and PVPh (0.2% by weight). However, the different vapor pressures of ethanol and EG cause nonuniform drying over a substrate. In addition, the contact angle of the ink on the substrate changed with nonuniform drying, because the contact angle (∼14°) of EG on silicon substrate is higher than that of ethanol (∼0°) and the portion of EG in the wet film increases during evaporation. Figure 2g illustrates the dewetting problem mainly caused by nonuniform drying. The lower evaporation rate of the mixture helps the 2D islands expand further, but irregular characteristics of the ink cause randomly distributed nanoparticle stacks, as shown in SEM images of panels h and i in Figure 2.

Using the same scalable wire-wound rod coating method, multilayer nanoparticle arrays can also be obtained by increasing the nanoparticle concentration in the ink. Figure 3a shows the relationship between the particle concentration and the number of nanoparticle layers formed after the solvent dries. When the nanoparticle concentration in-

DOI: 10.1021/nl101432r | *Nano Lett.* **2010,** *10,* 2989–2994

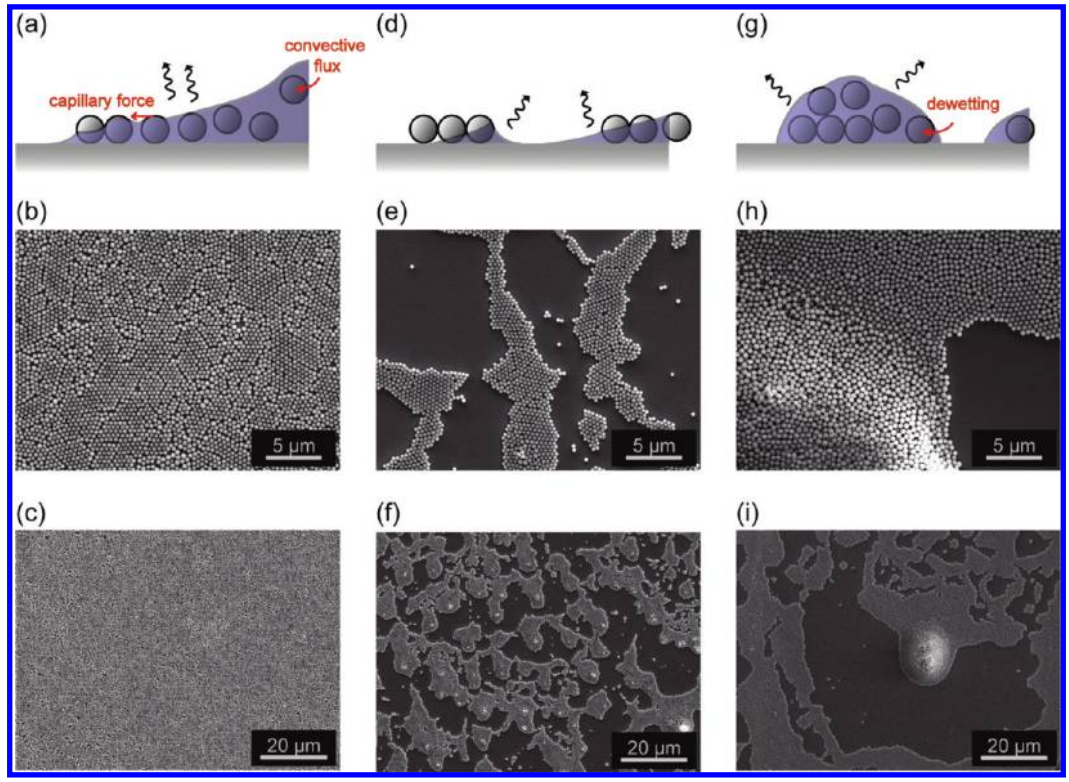

FIGURE 2. Schematic illustrations and SEM images of particle distribution after evaporation of (a−c) ethanol mixed with poly-4-vinylphenol, (d−f) ethanol only, and (g−i) ethanol mixed with ethylene glycol.

TABLE 1. The Evaporation Rate r (over 1.5 × 1.5 cm^2 in general lab conditions) and Viscosity μ of Tested Solvents

solvent	r (μg/s)	μ (cP)
EtOH only	164	1.07
EtOH + PVPh 0.2%	125	1.08
EtOH + PVPh 1%	97.1	1.28
EtOH + PVPh 5%	84.1	2.08
EtOH + PVPh 10%	73.5	4.06
EtOH + EG (1:1)	<10	6.89

creases from 50 to 100 to 200 g/L, the number of nanoparticle layers also proportionally increases from one to two to four, respectively. As shown in Figure 3b, double and four layers were formed over large areas, but their uniformities slightly decrease compared to the monolayer. For example, with the nanoparticle ink of a concentration of 200 g/L, 70% of the substrate is covered with four layers of nanoparticles and the remaining 30% is covered with three or five layers. Considering that a monolayer grows by the convective flux of nanoparticles, we can infer that if the nanoparticle concentration is higher, more particles flow to the boundary and start to form multiple layers. This concentration dependence was observed for both silicon and PET substrates.

These regular nanoparticle arrays on large area substrates can be used for various applications. As an example, we demonstrated that they can be used as substrates to improve light absorption in semiconductor thin films by reducing reflection and increasing scattering. The antireflection effect has already been demonstrated by several textured structures, such as nanodome-shaped solar cells[7] and silica sphere monolayers.[22,23] The scattering effect has been utilized mostly in metal nanoparticles.[24−26] Only a few results based on dielectric nanoparticles have been reported. However, dielectric nanoparticles with diameters comparable to the wavelength of incident light can have a strong Mie scattering effect.[27−29] This effect can be used for increasing the light path length and ultimately the absorption.

In order to test the absorption enhancement from dielectric nanoparticles, we deposited a thin film of a-Si:H on a silica nanoparticle monolayer. For this study, the monolayer of silica nanoparticles (100−600 nm in diameter) was coated on transparent soda-lime glass substrates. An oxygen plasma cleaning process (50 W, 2 min) was carried out to remove residual PVPh on the monolayer. Then an 80 nm thick indium tin oxide (ITO) layer was deposited by radio frequency (rf) sputtering at 80 W. This film transmitted 89% of all light between 400 and 800 nm, where a-Si:H absorbs. The a-Si:H layer was deposited by plasma-enhanced chemical vapor deposition (PECVD) at 250 °C and 60 W, followed by another 80 nm of ITO film deposited as before. In addition to reducing reflection, the large dielectric contrast between the ITO ($\epsilon = 3.3$)[30] and a-Si:H ($\epsilon = 19.6$)[31] helps confine light within the a-Si:H layer.[32] Figure 4a shows a top-view SEM image of a sample made from a 400 nm diameter nanoparticle monolayer. Parts b and c of Figure 4 are schematic illustrations of the structures without and with a silver (Ag) layer as a reflector, respectively.

DOI: 10.1021/nl101432r | *Nano Lett.* **2010,** *10,* 2989--2994

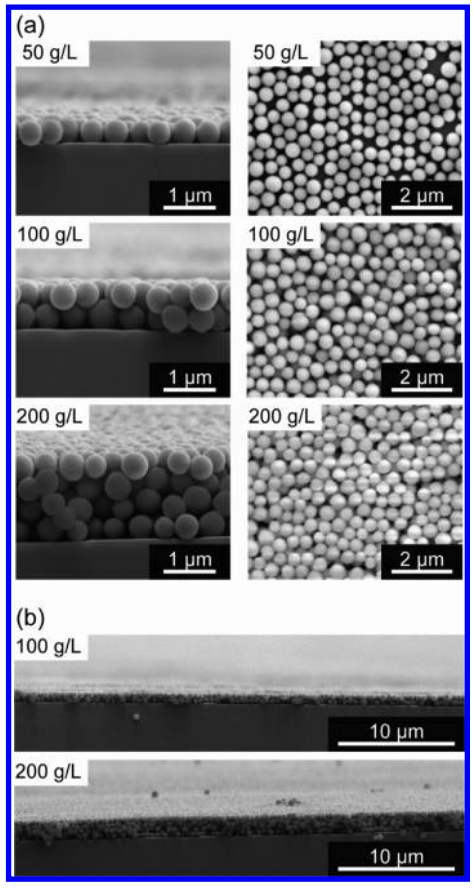

FIGURE 3. SEM images of silica nanoparticle distribution with different particle concentrations.

The structures in parts b and c of Figure 4 exhibit 40% and 68% enhanced light absorption compared to the flat film with the same thickness of materials, respectively, as shown in Figure 4d. The effective antireflection from the top surface and the scattered light from nanoparticles inside contribute to the improvement. It is noteworthy that both structures showed the same enhancement between 400 and 550 nm, which suggests the incoming light in this wavelength range was absorbed in a single pass through the structure and the enhancement comes from reduced reflection. However, beyond 550 nm, the light absorption for the two structures differs. The long wavelength light which cannot be absorbed in a single pass benefits from reflection at the Ag layer. The path length enhancement is especially strong beyond 730 nm, where the absorption length in a-Si:H is more than 10 μm.[33] For the optical simulation on the experimental device, we used the rigorous coupled-wave analysis (RCWA) algorithm. Figure 4e shows the light absorption data from the simulation, which was derived from the transmitted and reflected waves. The simulation result for the flat structure has many peaks over the 500 nm wavelength regime. Unlike the experimental device, the device geometry for the simulation has a perfectly flat interface, which causes the interference effect at the certain wavelength of light. The simulation data for the structures with nanoparticles do not have many narrow peaks but a couple of wide peaks over the 650 nm wavelength regime. The perfectly aligned nanostructure in the simulation devices has some grating effects on the light absorption, which create these peaks. Figure 4f shows the total absorption integrated over the Air Mass (AM) 1.5 solar spectrum in the range from 400 to 800 nm. Both nanostructured substrates showed much higher absorption (81% with the Ag back reflector and 73% without Ag) compared to the planar

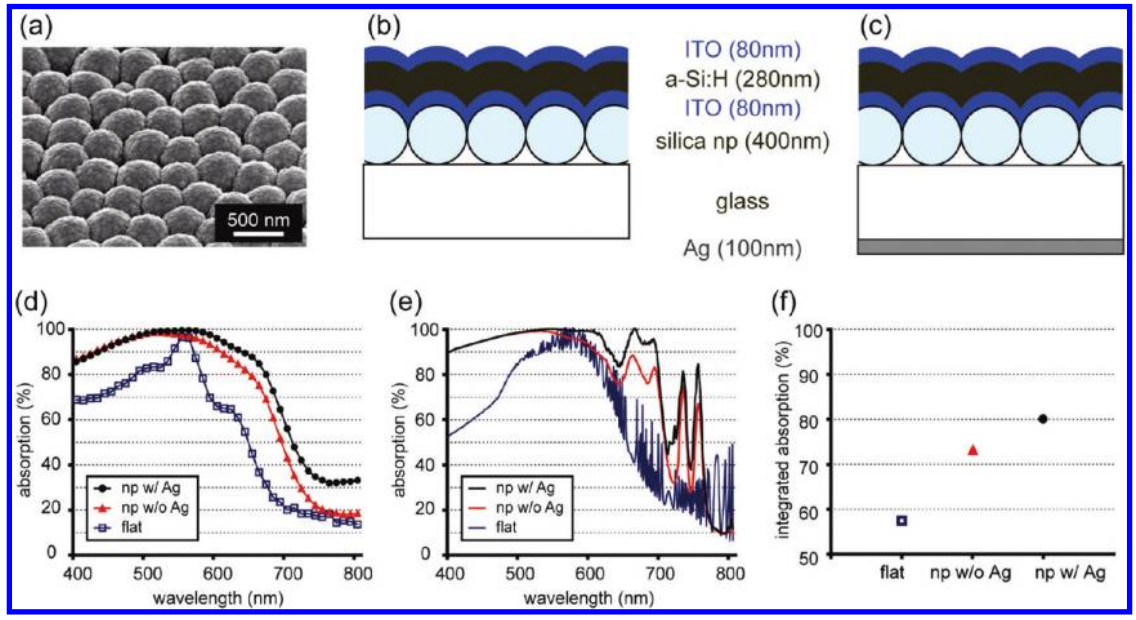

FIGURE 4. Light absorption measurements of thin a-Si:H films on silica nanoparticle monolayers. (a) A top-view SEM image. (b and c) Schematic illustrations of the cross section of structures without and with a silver layer, respectively, at the bottom. (d) Integrating sphere measurements of light absorption at normal incidence. (e) RCWA simulation of light absorption for flat and nanoparticle monolayer devices with and without Ag reflector. (f) The light absorption integrated over the AM 1.5 spectrum.

DOI: 10.1021/nl101432r | *Nano Lett.* **2010,** *10,* 2989–2994

control, which showed only 57% absorption even with the Ag back reflector. These results demonstrate that the nanoparticle monolayer structure is an effective light trapping template for photovoltaic applications.

The nanoparticle size is also a critical parameter in determining the light absorption. Small nanoparticles with diameters far below the wavelength of incident light are less effective at reducing reflection from the top surface. The nanodome shape, as shown in Figure 4a, results in the gradual change of refractive index from air to the absorber layer, leading to the effective antireflection effect. However, the shape of structures fabricated on small nanoparticle monolayers is less dome-shaped, but nearly flat to the incoming light. Larger particles, which have more pronounced dome shapes on the top surface, can also contribute to light trapping through Mie scattering. In order to see the nanoparticle size effect on thin-film absorption, we fabricated test samples with the structure shown in Figure 4c with the nanoparticle diameters between 100 and 600 nm, and Figure 5a shows their top-view SEM images. The structures with nanoparticle sizes of 100 and 220 nm showed lower absorption at every wavelength, as shown in Figure 5b, which is primarily due to higher reflection from the less textured surface. However, the 400 and 600 nm nanoparticle cases achieved the largest enhancements in the wavelength ranges of 550−670 and 670−800 nm, respectively. The enhancement factor is dependent on the particle size, which supports the Mie scattering enhancement mechanism. The integrated absorption over the AM 1.5 spectrum (400−800 nm wavelength) of each case is shown in Figure 5c. The larger nanoparticle case has higher light absorption, and it is mainly due to the difference of enhancement factor in the long wavelength range.

For another application, we demonstrated the enhanced hydrophobicity with a monolayer of nanoparticles. When a flat silicon substrate was modified with hydrophobic molecules, perfluorooctyltrichlorosilane (PFOS), by a vapor deposition method at room temperature for 1 h, the contact angle of a 2 μL water droplet was changed from zero to 98°, as shown in Figure 6a. However, when a monolayer of 400 nm silica nanoparticles was modified with the same method, the contact angle increased from 0 to 129°, as shown in Figure 6b. This result confirms that the wetting property of close-packed nanoparticles is well-described by the Cassie−Baxter model,[34] which assumes that the liquid forms a line of contact on the textured surface with air trapped below the contact line. Figure 6d is the illustration of wetting property of the nanoparticle monolayer, described by the Cassie−Baxter model, $\cos\theta_{CA} = f_1 \cos\theta_Y - f_2$, where θ_{CA} is the apparent contact angle, f_1 and f_2 are the area fractions of the solid/liquid and the air/liquid interface, and θ_Y is Young's contact angle.[35] On the basis of the data, $\theta_{CA}(129°)$ and $\theta_Y(98°)$, from this experiment, we can conclude that the contact line between water and air is below 70 nm from the top of silica nanoparticles. This textured surface of the

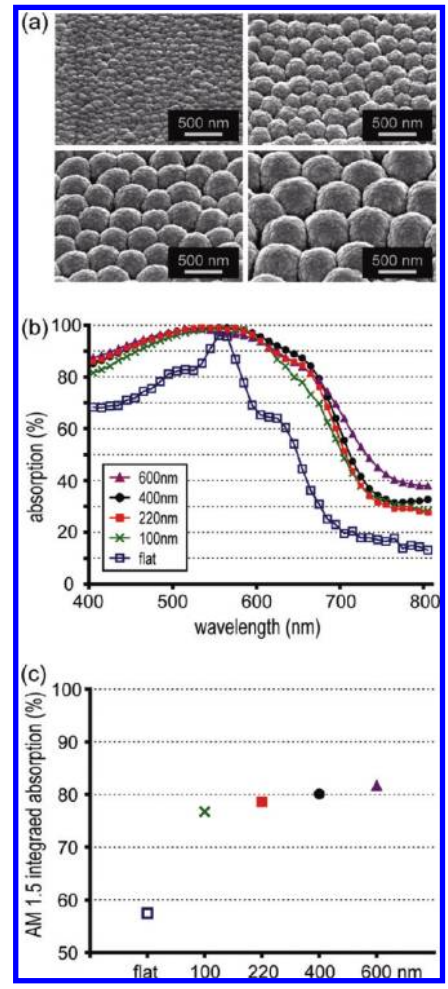

FIGURE 5. Light absorption measurements of thin a-Si:H films on different sizes of silica nanoparticle monolayers with the structure shown in Figure 4c: (a) top-view SEM images of samples on 100 (left top), 220 (right top), 400 (left bottom), and 600 nm (right bottom) nanoparticle monolayers; (b) integrating sphere measurement of light absorption at normal incidence; (c) the light absorption integrated over the AM 1.5 spectrum.

nanoparticle monolayer fabricated by the wire-wound rod method successfully increased the contact angle from 98° to 129°.

In conclusion, we have developed a simple and scalable printing method for assembling 2D and 3D close-packed nanoparticle arrays that is compatible with roll-to-roll processing on flexible substrates or assembly line coating on rigid substrates. Several parameters such as contact angle, solvent evaporation rate, and nanoparticle concentration have been studied to help understand the assembly mechanism. Thin films of a-Si:H deposited on these nanoparticle arrays showed up to a 42% increase in absorption over the integrated AM 1.5 spectrum compared to a planar control structure. This enhancement is attributed to reduced reflection and increased scattering resulting from regularly packed nanoparticles. In addition, the texturing made by the monolayer of nanoparticles increased the contact angle of a water droplet by 32%. This wire-wound rod method provides a

DOI: 10.1021/nl101432r | *Nano Lett.* **2010,** *10,* 2989–2994

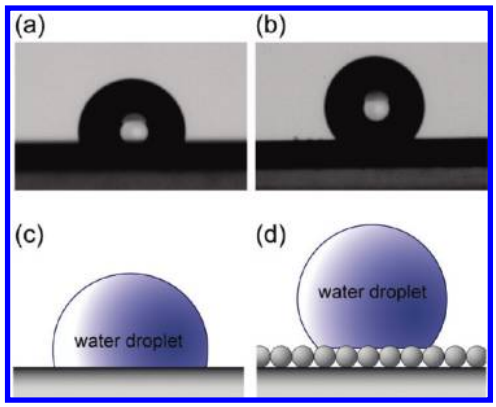

FIGURE 6. Optical micrographs and illustrations of a water droplet on two substrates after PFOS modification: (a) flat Si substrate with a contact angle of 98°; (b) monolayer of 400 nm silica nanoparticles on top of flat Si substrate with a contact angle of 129°; (c, d) illustrations of (a) and (b), respectively.

scalable path to implementing the extraordinary benefits of nanostructured substrates for solar and other applications.

Acknowledgment. Y.C. acknowledges support from U.S. Department of Energy under the Award Number DE-FG36-08GOI8004. S.J. and H.R.L. acknowledge support from the Korea Foundation for Advanced Studies (KFAS) and the Kwanjeong Educational Foundation (KEF) for graduate fellowships, respectively. We thank Ching-Mei Hsu and Dr. Zongfu Yu for very helpful discussions on the contact angle measurement experiment and the optical simulation, respectively.

Supporting Information Available. SEM images of silica nanoparticle distribution with different concentrations of PVPh. This material is available free of charge via the Internet at http://pubs.acs.org.

REFERENCES AND NOTES

(1) Tsakalakos, L.; Balch, J.; Fronheiser, J.; Korevaar, B. A.; Sulima, O.; Rand, J. *Appl. Phys. Lett.* **2007**, *91*, 233117.
(2) Kelzenberg, M. D.; Boettcher, S. W.; Petykiewicz, J. A.; Turner-Evans, D. B.; Putnam, M. C.; Warren, E. L.; Spurgeon, J. M.; Briggs, R. M.; Lewis, N. S.; Atwater, H. A. *Nat. Mater.* **2010**, *9*, 239–244.
(3) Garnett, E.; Yang, P. *Nano Lett.* **2010**, *10*, 1082–1087.
(4) Zhu, J.; Yu, Z.; Burkhard, G. F.; Hsu, C.; Connor, S. T.; Xu, Y.; Wang, Q.; McGehee, M.; Fan, S.; Cui, Y. *Nano Lett.* **2009**, *9*, 279–282.
(5) Sahoo, K. C.; Lin, M.; Chang, E.; Tinh, T. B.; Li, Y.; Huang, J. *Jpn. J. Appl. Phys.* **2009**, *48*, 126508.
(6) Yu, Z.; Gao, H.; Wu, W.; Ge, H.; Chou, S. Y. *J. Vac. Sci. Technol., B* **2003**, *21*, 2874–2877.
(7) Zhu, J.; Hsu, C.; Yu, Z.; Fan, S.; Cui, Y. *Nano Lett.* **2010**, *10*, 1979–1984.
(8) Fan, Z.; Razavi, H.; Do, J.; Moriwaki, A.; Ergen, O.; Chueh, Y.; Leu, P. W.; Ho, J. C.; Takahashi, T.; Reichertz, L. A.; Neale, S.; Yu, K.; Wu, M.; Ager, J. W.; Javey, A. *Nat. Mater.* **2009**, *8*, 648–653.
(9) Xia, F.; Jiang, L. *Adv. Mater.* **2008**, *20*, 2842–2858.
(10) Geim, A. K.; Dubonos, S. V.; Grigorieva, I. V.; Novoselov, K. S.; Zhukov, A. A.; Shapoval, S. Y. *Nat. Mater.* **2003**, *2*, 461–463.
(11) Sitti, M.; Fearing, R. S. *J. Adhes. Sci. Technol.* **2003**, *17*, 1055–1073.
(12) Huang, J.; Kim, F.; Tao, A. R.; Connor, S.; Yang, P. *Nat. Mater.* **2005**, *4*, 896–900.
(13) Hsu, C.; Connor, S. T.; Tang, M. X.; Cui, Y. *Appl. Phys. Lett.* **2008**, *93*, 133109–3.
(14) Jiang, P.; McFarland, M. J. *J. Am. Chem. Soc.* **2004**, *126*, 13778–13786.
(15) Tracton, A. A. *Coatings Technology Handbook*, 3rd ed.;CRC Press: Boca Raton, FL, 2005.
(16) Bogush, G.; Tracy, M.; Zukoski IV, C. *J. Non-Cryst. Solids* **1988**, *104*, 95–106.
(17) Denkov, N. D.; Velev, O. D.; Kralchevsky, P. A.; Ivanov, I. B.; Yoshimura, H.; Nagayama, K. *Nature* **1993**, *361*, 26.
(18) Kralchevsky, P. A.; Nagayama, K. *Langmuir* **1994**, *10*, 23–36.
(19) Adachi, E.; Dimitrov, A. S.; Nagayama, K. *Langmuir* **1995**, *11*, 1057–1060.
(20) Dimitrov, A. S.; Nagayama, K. *Langmuir* **1996**, *12*, 1303–1311.
(21) *Paint and coating testing manual*; Koleske, J. V., Ed.; ASTM International: Philadelphia, PA, 1995.
(22) Tao, M.; Zhou, W.; Yang, H.; Chen, L. *Appl. Phys. Lett.* **2007**, *91*, 081118–3.
(23) Wang, Y.; Tummala, R.; Chen, L.; Guo, L. Q.; Zhou, W.; Tao, M. *J. Appl. Phys.* **2009**, *105*, 103501–6.
(24) Beck, F. J.; Polman, A.; Catchpole, K. R. *J. Appl. Phys.* **2009**, *105*, 114310–7.
(25) Pillai, S.; Catchpole, K. R.; Trupke, T.; Green, M. A. *J. Appl. Phys.* **2007**, *101*, 093105–8.
(26) Derkacs, D.; Lim, S. H.; Matheu, P.; Mar, W.; Yu, E. T. *Appl. Phys. Lett.* **2006**, *89*, 093103–3.
(27) Mie, G. *Ann. Phys.* **1908**, *330*, 377–445.
(28) Scholz, S. M.; Vacassy, R.; Dutta, J.; Hofmann, H.; Akinc, M. *J. Appl. Phys.* **1998**, *83*, 7860–7866.
(29) Bohren, C. F.; Huffman, D. R. *Absorption and Scattering of Light by Small Particles*; Wiley-Interscience: New York, 1998.
(30) Christ, A.; Tikhodeev, S. G.; Gippius, N. A.; Kuhl, J.; Giessen, H. *Phys. Rev. Lett.* **2003**, *91*, 183901.
(31) Palik, E. D. *Handbook of Optical Constants of Solids*; Elsevier: Amsterdam, 1998.
(32) Hecht, E. *Optics*, 4th ed.; Addison Wesley: Reading, MA, 2001.
(33) Poruba, A.; Springer, J.; Mullerova, L.; Beitlerova, A.; Vanecek, M.; Wyrsch, N.; Shah, A. *J. Non-Cryst. Solids* **2004**, *338–340*, 222–227.
(34) Shiu, J.; Kuo, C.; Chen, P.; Mou, C. *Chem. Mater.* **2004**, *16*, 561–564.
(35) Cassie, A. B. D.; Baxter, S. *Trans. Faraday Soc.* **1944**, *40*, 546–551.

DOI: 10.1021/nl101432r | *Nano Lett.* **2010,** *10,* 2989–2994